PNAS

Supporting Information for
Driving forces of the complex formation between highly charged disordered proteins

Aritra Chowdhury[1], Alessandro Borgia[1,2], Souradeep Ghosh[3], Andrea Sottini[1], Soumik Mitra[3], Rohan Eapen[1], Madeleine B. Borgia[1,2], Tianjin Yang[1], Nicola Galvanetto[1,4], Miloš T. Ivanović[1], Pawel Lukijanczuk[1], Ruijing Zhu[1], Daniel Nettels[1], Arindam Kundagrami[3], Benjamin Schuler[1,4]

[1]Department of Biochemistry, University of Zurich, Zurich, 8057 Switzerland

[2]Current Address: Department of Structural Biology, St. Jude Children's Research Hospital, Memphis, TN 38105, USA

[3]Department of Physical Sciences and Centre for Advanced Functional Materials, Indian Institute of Science Education and Research Kolkata, Mohanpur 741246, India

[4]Department of Physics, University of Zurich, Zurich, 8057 Switzerland

Email: a.chowdhury@bioc.uzh.ch, arindam@iiserkol.ac.in, schuler@bioc.uzh.ch

This PDF file includes:

Supporting Text

Protein preparation and labeling

Recombinant human histone H1.0 produced in *E. coli* was from New England Biolabs (cat. # M2501S). Unlabeled ProTα (WT isoform 2) and ProTα 56C/110C (isoform 1), used for fluorescent labeling, were purified using His_6-tagged constructs as described previously[1-4]. ProTα 2C/110C (isoform 1) used for fluorescent labeling was either expressed and purified as a His_6-tagged construct as described previously or was cloned into a pBAD-IntCBD-12His vector and purified according to a previously described protocol[5]. Note that although His_6- or His_{12}-tags were used for purification by immobilized metal chelate affinity chromatography, the tags were subsequently removed in all cases by protease cleavage or thiol-induced self-cleavage of an intein[5] for His_6- and His_{12}-bearing proteins, respectively. See Table S3 for all protein sequences used in the measurements. For fluorescence labeling, 10-15 nmol of the purified protein were reduced with 10 mM Tris(2-carboxyethyl) phosphine hydrochloride (TCEP) for one hour in phosphate-buffered saline (PBS), pH 7, supplemented with 4 M guanidinium chloride (GdmCl) and 0.2 mM EDTA. Excess TCEP was removed subsequently via repeated (5x) buffer exchange using 3-kDa molecular weight cut off centrifugal concentrators with the labeling buffer (PBS pH 7, 4 M GdmCl, 0.2 mM TCEP and 0.2 mM EDTA). The protein was subsequently labeled with Alexa488-C5 maleimide and Alexa594-C5 maleimide (Invitrogen) using ~6.5-fold molar excess of both the dyes relative to protein at room temperature for one hour followed by overnight incubation at 4 °C. The unreacted dye was quenched with 10 mM dithiothreitol at room temperature for 10 minutes and removed subsequently by repeated buffer exchange with labeling buffer using centrifugal concentrators. The double-labeled protein was separated from the reaction mixture by RP-HPLC on a Reprosil Gold C18 column (Dr. Maisch, Germany), lyophilized, and stored at −80 °C. The integrity of all the samples was confirmed using electrospray ionization mass spectrometry.

Single-molecule spectroscopy

Single-molecule FRET experiments were performed on freely diffusing molecules with a MicroTime 200 confocal single-molecule instrument (PicoQuant, Berlin, Germany). The samples were excited with a 488-nm laser (Sapphire 488–100 CDRH, Coherent, Santa Clara, CA) through a high-numerical aperture water-immersion objective (Olympus UplanApo 60x/1.20 W). The fluorescence signal was spatially filtered using a 100-μm pinhole and split into donor and acceptor signals using a dichroic mirror (585DCXR, Chroma, Rockingham, VT); each component, after further spectral filtering using bandpass filters (Chroma ET525/50 M for donor signal and HQ650/100 for acceptor signal), was focused on an avalanche photodiode detector (SPCM-AQR-15, PerkinElmer Optoelectronics, Vaudreuil, QC, Canada). A HydraHarp 400 (PicoQuant, Berlin, Germany) was used to record individual photon arrival times from the detectors. Most experiments were performed with continuous-wave laser excitation. Temperature-dependent experiments were performed with pulsed interleaved excitation (PIE)[6], where the samples were excited with alternating pulses of the 488-nm laser and laser emission at 585 nm, obtained by spectrally filtering the output of a supercontinuum laser (EX-12 SuperK Extreme, NKT photonics); laser synchronization for PIE experiments was achieved with a Sepia II laser driver (PicoQuant, Berlin, Germany). All experiments were performed with 50-100 pM doubly labeled samples in 10 mM Tris buffer (pH 7.4), containing different concentrations of salts and sometimes additional additives, as stated in main text, supplemented with 0.01% Tween 20 to prevent surface adhesion of molecules and 140 mM β-mercaptoethanol as a photoprotectant. All experiments, except temperature-dependent measurements, were performed in chambered plastic cover slides (μ-Slide, ibidi, Germany) to minimize protein surface adhesion.

For temperature-dependent experiments, a custom-built sample holder allowing temperature control with a water-cooled Peltier element driven by a temperature controller (BelektroniG, Germany) was used[7]; the objective was heated and cooled with an aluminum collar containing a Peltier element driven by a temperature controller (BelektroniG, Germany). A glass cuvette was used for temperature measurements[7]. To prevent surface adhesion of protein molecules, the glass surface was coated with the amorphous fluoropolymer CYTOP (CTX-809AP2, solvent CT-SOLV180, AGC Chemicals Europe, Thornton-Cleveleys, United Kingdom)[8]. The cylinder and the bottom glass coverslip of the cuvette were first cleaned by boiling with 2% Deconex® INSTRUMENT PLUS (Borer Chemie AG, Zuchwil, Switzerland) solution and double-distilled water, and subsequently plasma-oxidized (Femto 1A, Diener electronic, Ebhausen, Germany) for 60 seconds at 25% power. The surfaces of the glass cylinder and the coverslip were modified with (3-aminopropyl)-triethoxysilane (APTES, Sigma-Aldrich, Buchs, Switzerland) with a 5% v/v ethanolic APTES solution for 30 minutes. Unreacted APTES was removed by rinsing the cylinder and the coverslip with ethanol followed by drying with compressed air. The glass slide was spin-coated with CYTOP solution (9% w/v) at 900 rpm, achieving a coating thickness of ~4 µm. The cylinder was dip-coated in the CYTOP solution (9% w/v). Afterwards, the cylinder and glass slide were placed on a hot plate set to 70 °C for 30 minutes to let the solvent evaporate. Finally, the cylinder and the coverslip were aligned and thermally bonded for 2 hours at 180 °C, above the glass transition temperature of CYTOP. For some temperature-dependent experiments, a customized 3D-printed cuvette using a photoreactive poly-urethane resin (UltraCur3D RG35 from BASF, Germany) was used, with comparable results. The temperature in the confocal volume was calibrated via the temperature-dependent fluorescence lifetime of Rhodamine B[7,9].

From the fluorescence recordings of freely diffusing single molecules, transfer efficiencies from the selected photon bursts (≥3000 bursts for each measurement), each originating from a single molecule traversing the confocal volume, were quantified according to $E = n_{\mathrm{A}}/(n_{\mathrm{D}} + n_{\mathrm{A}})$, where n_{D} and n_A are the numbers of donor and acceptor photons, respectively, following donor excitation in a given burst, corrected for background, spectral crosstalk between channels, acceptor direct excitation, and differences in dye quantum yields and detection efficiencies[10]. For PIE experiments, stoichiometry ratios were additionally calculated from every burst according to $S = (n_{\mathrm{D}} + n_{\mathrm{A}})/(n_{\mathrm{D}} + n_{\mathrm{A}} + n_{\mathrm{A}}^{\mathrm{A}})$, where $n_{\mathrm{A}}^{\mathrm{A}}$ is the number acceptor photons following acceptor excitation in a given burst, corrected for background signal and different donor and acceptor laser excitation intensities[10]. Data analysis was performed with Fretica, a custom add-on for Mathematica (Wolfram Research) available at https://github.com/SchulerLab.

Binding affinity from single-molecule experiments

We employed single-molecule FRET using double-labeled ProTα (P*) to measure the dissociation constants $K_{\mathrm{D}}^{\mathrm{PH}}$, $K_{\mathrm{D}}^{\mathrm{PPH}}$, and $K_{\mathrm{D}}^{\mathrm{PHH}}$ for the following equilibria:

$$\mathrm{P} + \mathrm{H} \overset{K_{\mathrm{D}}^{\mathrm{PH}}}{\rightleftharpoons} \mathrm{PH} \qquad \text{eq.1}$$

$$\mathrm{PH} + \mathrm{P} \overset{K_{\mathrm{D}}^{\mathrm{PPH}}}{\rightleftharpoons} \mathrm{PPH} \qquad \text{eq.2}$$

$$\mathrm{PH} + \mathrm{H} \overset{K_{\mathrm{D}}^{\mathrm{PHH}}}{\rightleftharpoons} \mathrm{PHH} \qquad \text{eq.3}$$

For measuring $K_{\mathrm{D}}^{\mathrm{PH}}$, we titrated 50-70 pM P* with increasing amounts of unlabeled H1, and the series of transfer efficiency histograms was fitted globally with a sum of two Gaussian peak functions of independent amplitudes but shared positions and widths among the histograms.

The areas of the two peaks are proportional to the concentrations, $c_{\mathrm{P^*H}}$ and $c_{\mathrm{P^*}}$, of bound and unbound P*, respectively, allowing us to quantify the fraction of heterodimer, $\theta_{\mathrm{PH}} = \frac{c_{\mathrm{P^*H}}}{c_{\mathrm{P^*}}+c_{\mathrm{P^*H}}}$, as a function of the total H1 concentration added, $c_{\mathrm{H}}^{\mathrm{tot}}$. Fitting these measured fractions with

$$\theta_{\mathrm{PH}}(c_{\mathrm{H}}^{\mathrm{tot}}) = \frac{\left(c_{\mathrm{H}}^{\mathrm{tot}} + K_{\mathrm{D}}^{\mathrm{PH}} + c_{\mathrm{P^*}}^{\mathrm{tot}}\right) - \sqrt{\left(c_{\mathrm{H}}^{\mathrm{tot}} + K_{\mathrm{D}}^{\mathrm{PH}} + c_{\mathrm{P^*}}^{\mathrm{tot}}\right)^2 - 4c_{\mathrm{H}}^{\mathrm{tot}}c_{\mathrm{P^*}}^{\mathrm{tot}}}}{2c_{\mathrm{P^*}}^{\mathrm{tot}}}, \qquad \text{eq.4}$$

where $c_{\mathrm{P^*}}^{\mathrm{tot}}$ is the known total P* concentration, yields $K_{\mathrm{D}}^{\mathrm{PH}}$. For temperature-dependent measurements, the bound fraction was measured for a given concentration of H1 at different temperatures, and the temperature-dependent values of $K_{\mathrm{D}}^{\mathrm{PH}}$ were obtained by solving eq. 4 for $K_{\mathrm{D}}^{\mathrm{PH}}$. At very low salt concentrations and in presence of osmolytes, eq. 4 was insufficient for fitting the binding isotherms owing to surface adhesion of H1, so in those cases, we applied a model that accounts for the competition between ProTα binding and surface adhesion of H1.[2]

$K_{\mathrm{D}}^{\mathrm{PHH}}$ was estimated in a similar way as $K_{\mathrm{D}}^{\mathrm{PH}}$: We formed P*H by mixing 50-70 pM P* with 3 nM unlabeled H1, a concentration much greater than $K_{\mathrm{D}}^{\mathrm{PH}}$ at the monovalent salt concentrations where these measurements were performed (~8-80 mM), and titrated the sample with increasing amounts of unlabeled H1. The resulting series of transfer efficiency histograms with two peaks corresponding to P*H and P*HH, were globally fitted as described above. From the relative areas under the peaks, we obtain the fraction $\theta_{\mathrm{PHH}} = \frac{c_{\mathrm{P^*HH}}}{c_{\mathrm{P^*H}}+c_{\mathrm{P^*HH}}}$ as a function of the excess H1 concentration, $c_{\mathrm{H}}^{\mathrm{ex}}$, which is given by the difference between total H1 concentration added, $c_{\mathrm{H}}^{\mathrm{tot}}$, and the initial P*H concentration, $c_{\mathrm{P^*H}}^{\mathrm{ini}}$. At the monovalent salt concentrations used, $K_{\mathrm{D}}^{\mathrm{PH}}$ is sub-picomolar, and PH is fully formed, with negligible concentrations of unbound P* remaining, thus we assume $c_{\mathrm{P^*H}}^{\mathrm{ini}} = c_{\mathrm{P^*}}^{\mathrm{tot}}$ (the total P* concentration). Since $c_{\mathrm{H}}^{\mathrm{tot}} \gg c_{\mathrm{P^*H}}^{\mathrm{ini}}$, we assume $c_{\mathrm{H}}^{\mathrm{ex}} \approx c_{\mathrm{H}}^{\mathrm{tot}}$, and fitting the measured fractions with

$$\theta_{\mathrm{PHH}}(c_{\mathrm{H}}^{\mathrm{tot}}) = \frac{\left(c_{\mathrm{H}}^{\mathrm{tot}} + K_{\mathrm{D}}^{\mathrm{PHH}} + c_{\mathrm{P^*H}}^{\mathrm{ini}}\right) - \sqrt{\left(c_{\mathrm{H}}^{\mathrm{ex}} + K_{\mathrm{D}}^{\mathrm{PHH}} + c_{\mathrm{P^*H}}^{\mathrm{ini}}\right)^2 - 4c_{\mathrm{H}}^{\mathrm{ex}}c_{\mathrm{P^*H}}^{\mathrm{ini}}}}{2c_{\mathrm{P^*H}}^{\mathrm{ini}}} \qquad \text{eq.5}$$

yields $K_{\mathrm{D}}^{\mathrm{PHH}}$.

$K_{\mathrm{D}}^{\mathrm{PPH}}$ was estimated via a competition experiment where 10 nM unlabeled ProTα and H1 (P and H, respectively) doped with 50 pM P* were titrated with increasing concentrations of P at low monovalent salt concentration (~65-110 mM). Since the affinities of labeled and unlabeled ProTα for H1 are very similar[1], we assume that P* partitions equally into all ProTα-containing species and represents their relative equilibrium populations. The resulting series of transfer efficiency histograms were globally fitted as above, but now with a sum of three Gaussian peak functions for P*, P*H, and P*PH; the areas of the peaks are proportional to their respective concentrations, $c_{\mathrm{P^*}}$, $c_{\mathrm{P^*H}}$, and $c_{\mathrm{P^*PH}}$, allowing us to quantify the fraction $\theta_{\mathrm{PPH}} = \frac{c_{\mathrm{P^*PH}}}{c_{\mathrm{P^*PH}}+c_{\mathrm{P^*H}}}$ as a function of the excess ProTα concentration, $c_{\mathrm{P}}^{\mathrm{ex}}$, which is the difference between the total ProTα concentration, $c_{\mathrm{P}}^{\mathrm{tot}}$, and the initial PH concentration, $c_{\mathrm{PH}}^{\mathrm{ini}}$. At the low salt concentrations used, $K_{\mathrm{D}}^{\mathrm{PH}}$ is sub-picomolar, PH is fully formed, and its initial concentration, $c_{\mathrm{PH}}^{\mathrm{ini}}$, is thus equal to 10 nM. Fitting the measured fractions with

$$\theta_{\mathrm{PPH}}(c_{\mathrm{P}}^{\mathrm{ex}}) = \frac{\left(c_{\mathrm{P}}^{\mathrm{ex}} + K_{\mathrm{D}}^{\mathrm{PPH}} + c_{\mathrm{PH}}^{\mathrm{ini}}\right) - \sqrt{\left(c_{\mathrm{P}}^{\mathrm{ex}} + K_{\mathrm{D}}^{\mathrm{PPH}} + c_{\mathrm{PH}}^{\mathrm{ini}}\right)^2 - 4c_{\mathrm{P}}^{\mathrm{ex}}c_{\mathrm{PH}}^{\mathrm{ini}}}}{2c_{\mathrm{PH}}^{\mathrm{ini}}}, \qquad \text{eq.6}$$

yields $K_{\mathrm{D}}^{\mathrm{PPH}}$. For all affinities measured by single-molecule FRET, we conservatively quote an error of a factor 2 in K_{D} (corresponding to ±0.7 k_{B}T in binding free energy), based on the variance previously observed for K_{D} measurements from repeat experiments and the variance of different dye pairs and labeling positions[1]. We note that ProTα by itself remains monomeric up to a concentration of at least 5 mg/mL according to scattering experiments[11].

ProTα dimensions and associated configurational entropy change estimated from single-molecule FRET

Single-molecule FRET of the terminally labeled (2C/110C) variant of ProTα was used to estimate average root-mean-square (RMS) end-to-end distances. Transfer efficiency histograms measured at different concentrations of KCl and in the absence and presence of H1 were fitted with a Gaussian peak function to estimate the corresponding mean transfer efficiencies $\langle E \rangle$, from which the RMS distances were inferred using the relation

$$\langle E \rangle = \int_0^\infty P(r)E(r)dr\,, \qquad \text{eq.7}$$

where $P(r)$ is a distance probability density function, and $E(r)$ is given by

$$E(r) = R_0^6/(R_0^6 + r_0^6)\,, \qquad \text{eq.8}$$

where the Förster radius R_0 is 5.4 nm for Alexa 488 and 594 in water and was corrected for the refractive index of the solution (using the known dependence of refractive index on KCl concentration)[12]. We used the empirically modified self-avoiding random walk model (SAW-ν) for $P(r)$[13]. The length scaling exponent, *ν*, was obtained for the 2-110 segment of ProTα by accounting for the total length of both linkers and fluorophores equivalent to 9 amino acids[14]. Finally, the average end-to-end distance of the entire ProTα chain (R_e) was estimated using the value of *ν* obtained and the number of peptide bonds (110 for ProTα). We approximate the change in free energy due to the change in configurational entropy of ProTα upon binding H1, ΔG_{conf}, by assuming $P(r)$ for a Gaussian chain, as

$$\frac{\Delta G_{conf}}{k_{\mathrm{B}}T} = \ln\frac{R_{e,u}}{R_{e,b}}, \qquad \text{eq.9}$$

where $R_{e,u}$ and $R_{e,b}$ are the average root-mean-square end-to-end distances for unbound and H1-bound ProTα, respectively[15].

Salt and osmolyte dependences of H1-ProTα binding

In the presence of a salt of monovalent cations and anions, n_- anions (A^-) and n_+ cations (C^+) associated with the individual proteins are released upon H1-ProTα binding[16]:

$$\mathrm{ProT\alpha} + \mathrm{H1} \rightleftharpoons \mathrm{ProT\alpha\text{-}H1} + n_+\mathrm{C}^+ + n_-\mathrm{A}^-. \qquad \text{eq.10}$$

For binding in the presence of a salt of monovalent cations and divalent anions (A^{2-}), we have:

$$\mathrm{ProT\alpha} + \mathrm{H1} \rightleftharpoons \mathrm{ProT\alpha\text{-}H1} + n_+\mathrm{C}^+ + n_{2-}\mathrm{A}^{2-}, \qquad \text{eq.11}$$

and in the presence of a salt of monovalent anions and divalent cations (C^{2+}),

$$\mathrm{ProT\alpha} + \mathrm{H1} \rightleftharpoons \mathrm{ProT\alpha\text{-}H1} + n_{2+}\mathrm{C}^{2+} + n_-\mathrm{A}^-\,, \qquad \text{eq.12}$$

where n_{2+} and n_{2-} denote the numbers of released divalent cations and anions, respectively.

One can relate the dependence of the observed equilibrium dissociation constant for H1-ProTα binding, $K_{\mathrm{D}}^{\mathrm{PH}}$, as a function of the mean ionic activity of a given salt to the number of ions released upon H1 binding to ProTα[2,16]. The respective relations for different salts, either

with monovalent cations and anions (LiCl, KCl, CsCl), with divalent cation and monovalent anion ($MgCl_2$), and with monovalent cation and divalent anions (K_2SO_4) are given by

$$n_+ + n_- = n_{\mathrm{mono}} = \frac{d \log K_{\mathrm{D}}^{\mathrm{PH}}}{d \log a_\pm} \qquad \text{eq.13}$$

$$n_{2+} + n_- = n_{\mathrm{di-cat}} = \frac{d \log K_{\mathrm{D}}^{\mathrm{PH}}}{d \log a_\pm} \qquad \text{eq.14}$$

$$n_+ + n_{2-} = n_{\mathrm{di-an}} = \frac{d \log K_{\mathrm{D}}^{\mathrm{PH}}}{d \log a_\pm}, \qquad \text{eq.15}$$

where $a_\pm$ is the mean ionic activity calculated as described below (eq. 16). If we assume that the number of charges released upon H1-ProTα binding is independent of the type of salt used, and that an equal number of positive and negative charges are released, i.e., $n_+ = n_-$, $n_{2+} = \frac{1}{2} n_+$, and $n_{2-} = \frac{1}{2} n_-$, we obtain $n_{\mathrm{di-cat}} = n_{\mathrm{di-an}} = 0.75\, n_{\mathrm{mono}}$. The dependence of $K_{\mathrm{D}}^{\mathrm{PH}}$ on mean ionic activity for the different salts was analyzed globally using eqs. (13-15) after substituting $n_{\mathrm{di-cat}}$ and $n_{\mathrm{di-an}}$ with $0.75\, n_{\mathrm{mono}}$ in eqs. (14-15), with n_{mono} as a shared parameter for all data sets.

The mean ionic activity, $a_\pm$, for a molal concentration, m, of a salt is given by

$$a_\pm = m_\pm \gamma_\pm, \qquad \text{eq.16}$$

where $m_\pm$ is the mean ionic molality given by $m_\pm = m \left(v_+^{v_+} v_-^{v_-}\right)^{\frac{1}{(v_+ + v_-)}}$; v_+ and v_- are the stoichiometric coefficients of the cation and the anion, respectively; and $\gamma_\pm$ is the mean ionic activity coefficient[17]. The tabulated concentration dependences of $\gamma_\pm$ for the different salts[12] were interpolated with empirical equations (See Table S4 and Fig. S5) to obtain values of $a_\pm$ for all salt concentrations used. Note that at the low salt concentrations we used, molar and molal concentrations are virtually indistinguishable, and hence the former was used as a proxy for the latter.

The water activity, a_w, was varied with the neutral osmolyte triethylene glycol[18] (over a range of ~5-15% v/v) and quantified by vapor pressure osmometry (Vapro, ELITechGroup, France). a_w is related to the measured osmolality, m_s, by[19]

$$a_w = \exp(-m_s M_w), \qquad \text{eq.17}$$

where M_w is the molar mass of pure water.

Isothermal titration calorimetry (ITC)

ITC experiments were performed with a MicroCal iTC200 calorimeter (Malvern, UK) in 10 mM Tris buffer (pH 7.4) containing different concentrations of potassium chloride to attain different monovalent salt concentrations. For every salt concentration, two titrations were performed: H1 (H) was titrated with ProTα (P) and *vice versa*. A ~250-μM stock solution of the proteins was dialyzed against 150 mL of the measurement buffer overnight to equilibrate the samples with the same buffer. For the titrations, the titrand concentration in the ITC cell was kept between 15 and 25 μM, and the titrant concentration in the syringe was between 150 and 250 μM. To estimate the sample concentration loss due to surface adhesion, the titrant concentration was measured in the unused solution in the syringe after completion of the experiment, and the titrand concentration was measured before starting the titration by aspirating excess solution from the sample cell after cell loading was complete. Protein concentrations were measured spectrophotometrically on a Nanodrop (Thermo Scientific),

using an extinction coefficient of 3840 $M^{-1}cm^{-1}$ at 280 nm for H1 and extinction coefficients of 89,508 and 33,636 $M^{-1}cm^{-1}$ for ProTα at 215 nm and 225 nm, respectively[11].

Since ITC experiments are conducted in overfill mode, there is a volume displacement with every injection of the titrant that has to be accounted for to obtain accurate titrant and titrand concentrations in the cell, c_t and c_d, respectively, at any point of the injection sequence[20,21]:

$$c_{\mathrm{d}} = c_{\mathrm{d}}^{0}\left(\frac{2V_0 - \Delta V}{2V_0 + \Delta V}\right) \qquad \text{eq.18}$$

$$c_{\mathrm{t}} = c_{\mathrm{t}}^{0}\left(\frac{2\Delta V}{\Delta V + 2V_0}\right), \qquad \text{eq.19}$$

where c_{d}^{0} is the initial titrand concentration in the cell, c_{t}^{0} is the initial titrant concentration in the syringe, V_0 is the cell volume, and ΔV is the total displaced volume after n injections, $\Delta V = \sum_{i=1}^{n} V_i$, where V_i is the volume of the i^{th} injection. Complexation between P and H involves the three binding equilibria given by eqs. 1-3, associated with the molar enthalpy changes ΔH^{PH}, ΔH^{PPH}, and ΔH^{PHH}, respectively. The total heat absorbed cumulatively by the solution relative to unbound P and H after the i^{th} injection is

$$Q(i) = V_0\left[c_{\mathrm{PH}}\Delta H^{\mathrm{PH}} + c_{\mathrm{PPH}}\left(\Delta H^{\mathrm{PH}} + \Delta H^{\mathrm{PPH}}\right) + c_{\mathrm{PHH}}\left(\Delta H^{\mathrm{PH}} + \Delta H^{\mathrm{PHH}}\right)\right], \qquad \text{eq.20}$$

where c_{PH}, c_{PPH}, and c_{PHH} are the concentrations of PH, PPH, and PHH, respectively, in the cell after the i^{th} injection. The reaction heat of the i^{th} injection, $\Delta Q(i)$, normalized by the molar amount of titrant injected, Δn_t, is given by

$$\frac{\Delta Q(i)}{\Delta n_t} = \frac{Q(i) - Q(i-1) + \frac{V_i}{V_0}\left(\frac{Q(i) + Q(i-1)}{2}\right)}{c_{\mathrm{t}}^{0} V_i}, \qquad \text{eq.21}$$

where V_i is the volume of the i^{th} injection[21]. To calculate the ITC thermograms, we first calculated c_{PH}, c_{PPH}, and c_{PHH} for given total concentrations of P, $c_{\mathrm{P}}^{\mathrm{tot}}$, and H, $c_{\mathrm{H}}^{\mathrm{tot}}$, by solving the system of eqs. 22-26 numerically

$$K_{\mathrm{D}}^{\mathrm{PH}} = \frac{c_{\mathrm{P}} c_{\mathrm{H}}}{c_{\mathrm{PH}}} \qquad \text{eq.22}$$

$$K_{\mathrm{D}}^{\mathrm{PPH}} = \frac{c_{\mathrm{PH}} c_{\mathrm{P}}}{c_{\mathrm{PPH}}} \qquad \text{eq.23}$$

$$K_{\mathrm{D}}^{\mathrm{PHH}} = \frac{c_{\mathrm{PH}} c_{\mathrm{H}}}{c_{\mathrm{PHH}}} \qquad \text{eq.24}$$

$$c_{\mathrm{P}}^{\mathrm{tot}} = c_{\mathrm{P}} + c_{\mathrm{PH}} + 2c_{\mathrm{PPH}} + c_{\mathrm{PHH}} \qquad \text{eq.25}$$

$$\mathrm{c}_{\mathrm{H}}^{\mathrm{tot}} = \mathrm{c}_{\mathrm{H}} + \mathrm{c}_{\mathrm{PH}} + \mathrm{c}_{\mathrm{PPH}} + 2\mathrm{c}_{\mathrm{PHH}} \qquad \text{eq.26}$$

with respect to c_P, c_H, c_{PH}, c_{PPH}, and c_{PHH} for given values of $K_{\mathrm{D}}^{\mathrm{PH}}$, $K_{\mathrm{D}}^{\mathrm{PPH}}$, $K_{\mathrm{D}}^{\mathrm{PHH}}$, $c_{\mathrm{P}}^{\mathrm{tot}}$, and $c_{\mathrm{H}}^{\mathrm{tot}}$. c_P and c_H are the concentrations of free P and H, respectively. The result allowed us to calculate the thermograms using eqs. 18-21. The calculated $\frac{\Delta Q(i)}{\Delta n}$ values were fitted to the experimental ones by minimizing the residual sum of squares using a Nelder-Mead simplex algorithm in Mathematica (Wolfram Research). ΔH^{PH}, ΔH^{PPH}, ΔH^{PHH}, $K_{\mathrm{D}}^{\mathrm{PH}}$, $K_{\mathrm{D}}^{\mathrm{PPH}}$, $K_{\mathrm{D}}^{\mathrm{PHH}}$ are adjustable parameters for minimization. We allow for a ±20% uncertainty on titrant and titrand concentrations (instead of an uncertainty on stoichiometry) and for an offset between experimental and calculated $\frac{\Delta Q(i)}{\Delta n}$ to correct for non-specific heats[22,23]. The binding free energies were constrained to within an interval of ±1.5 $k_{\mathrm{B}}T$ of the values extrapolated from the

single-molecule measurements (Fig. S2) to account for the uncertainty of these values; the offset between the experimental and the calculated $\frac{\Delta Q(i)}{\Delta n}$ values was constrained to within an interval of ±3 kcal mol^{-1} (±12.6 kJ mol^{-1}), and the heat evolved for the last injection was subtracted from the thermograms before quantifying $\frac{\Delta Q(i)}{\Delta n}$ values. To fit the thermograms with a two-state binding model involving only the binding equilibrium given by eq. 1, the analogous approach was used, but with

$$Q(i) = \frac{V_0\,\Delta H^{\mathrm{PH}}}{2}\left[c_{\mathrm{H}}^{\mathrm{tot}} + c_{\mathrm{P}}^{\mathrm{tot}} + K_{\mathrm{D}}^{\mathrm{PH}} - \sqrt{(c_{\mathrm{P}}^{\mathrm{tot}} - c_{\mathrm{H}}^{\mathrm{tot}})^2 - 2(c_{\mathrm{P}}^{\mathrm{tot}} + c_{\mathrm{H}}^{\mathrm{tot}})K_{\mathrm{D}}^{\mathrm{PH}} + (K_{\mathrm{D}}^{\mathrm{PH}})^2}\right] \quad \text{eq.27}$$

instead of eq. 20. Subsequently, as in the previous case, the calculated $\frac{\Delta Q(i)}{\Delta n}$ values were fitted to experimental ones by minimizing the residual sum of squares with ΔH^{PH} and $K_{\mathrm{D}}^{\mathrm{PH}}$ as adjustable parameters, allowing for a 20% error on titrant and titrand concentrations, and an offset between the experimental and calculated $\frac{\Delta Q(i)}{\Delta n}$. For the enthalpies from the thermogram fits, we use a conservative estimate of the uncertainty of ±20% of the resulting values, given that we allow for a 20% error on titrant and titrand concentrations.

Analysis of the temperature-dependent ProTα-H1 affinity with single-molecule FRET

The temperature dependence of $K_{\mathrm{D}}^{\mathrm{PH}}$ from the single-molecule FRET measurements at different salt concentrations was fitted with the integrated form of the Van 't Hoff equation[24],

$$ln\frac{K_{\mathrm{D}}^{\mathrm{PH}}(T_0)}{K_{\mathrm{D}}^{\mathrm{PH}}(T)} = \frac{\Delta H^{\mathrm{PH}}(T_0) - T_0\Delta C_{\mathrm{p}}}{R}\left(\frac{1}{T_0} - \frac{1}{T}\right) + \frac{\Delta C_{\mathrm{p}}}{R}\,ln\frac{T}{T_0}, \quad \text{eq.28}$$

where R is the universal gas constant, $K_{\mathrm{D}}^{\mathrm{PH}}(T)$ is the equilibrium dissociation constant at absolute temperature T; $\Delta H^{\mathrm{PH}}(T_0)$ and $K_{\mathrm{D}}^{\mathrm{PH}}(T_0)$ are the corresponding values at the reference temperature T_0, and ΔC_{p} is the change in heat capacity upon binding. Using $\Delta H^{\mathrm{PH}}(T_0)$, with T_0 = 276K, directly from the ITC measurements or from a linear interpolation of ΔH^{PH} as a function of salt concentration, we fitted all data sets globally with ΔC_{p} as a shared fit parameter.

Theory for complexation between two flexible polyelectrolytes

Free energy of two oppositely charged partially ionized interacting IDPs of different lengths

The theoretical framework we adapt here for complex formation between H1 and ProTα was previously described[25,26] and is based on the Edwards Hamiltonian[27] extended by Muthukumar for Coulomb interactions[28-30]; hence we provide only a short summary and mention the required modifications here. A dilute solution of volume Ω contains the two oppositely charged IDPs (ProTα and H1), which are modeled as flexible polyions[25,26,29,31] with their respective counterions and added salt. The polyions have different lengths and are partially ionized (only a fraction of the monomers are charged), with the ionizable monomers uniformly distributed along the chains[26]. The polyanion (PA) and polycation (PC) consist of N_1 and N_2 monomers, respectively, of which N_{c1} and N_{c2} are ionizable, respectively. There are N_{c1} and N_{c2} countercations and counteranions, respectively, that make the system electroneutral. All charges are assumed to be monovalent. At any time during the complexation process between the two chains, let n be the number of ionizable PA monomers, as well as PC monomers, that form the intermediate complex, which is thus taken to be electroneutral. The complexation process continues until all ionizable PA monomers are neutralized by PC monomers (for our purpose, the PA is assumed to contain fewer ionizable monomers than the PC, i.e. $N_{c1}<N_{c2}$, and consequently $n = N_{c1}$. The maximum degree of ionization is $f_{mi} = N_{ci}/N_i$, where i = 1, 2

indicate the PA and the PC, respectively, implying that $n_i = n/f_{mi}$ is the total number of monomers in the intermediate complex from the i^{th} chain.

In the intermediate state, M_i out of N_{ci} counterions remain condensed on the uncomplexed parts of the PA and PC, so the degrees of ionization of the uncomplexed parts are $f_i = (N_i f_{mi} - M_i - n)/\big(N_i - (n/f_{mi})\big)$. Let c_s be the number density of an added monovalent salt that dissociates into n_+ cations and n_- anions, where $c_s = n_+/\Omega = n_-/\Omega \equiv n_s/\Omega$. Therefore, $N_{ci} - M_i + n_s$ $(i = 1, 2)$ cations and anions, respectively, remain free in solution. The degree of counterion condensation for the uncomplexed chain parts is defined by $\alpha_i' = M_i/\big(N_i - (n/f_{mi})\big)$, which gives $f_i = f_{mi} - \alpha_i'$. The degree of ionization of the entire polyion (including both the complexed and uncomplexed parts) may be defined as $f_{Ti} = f_{mi} - M_i/N_i - n/N_i$, with the corresponding set of new variables related to α_i', which are $\alpha_i = M_i/(f_{mi}N_i - n) = \alpha_i'/f_{mi}$.

We consider the total free energy of the system[25,26] with the intermediate complex of n mutually bound, ionizable monomer pairs and $n_i(= n/f_{mi})$ total (ionizable as well as neutral) monomers from each polyion i, the counterions, and the implicit solvent. For each of the uncomplexed chain parts, M_i counterions are distributed within a volume for which the outer boundary is a cylinder of radius $d_c = \ell/4 + r_c$, and the inner boundary is set by the segment length along the chain (Fig. S3A), where ℓ is the Kuhn length, and r_c is the counterion diameter. The cylinder radius is set so that a counterion on the chain contour can be accommodated; thus, although $\ell/4$ seems counterintuitive as opposed to $\ell/2$, this discrepancy arises from the difference between the Kuhn length and segment length, necessitating a renormalization of the degree of polymerization and the effective length scale (see the following section). The translational entropy of counterions condensed on the polyions leads to the free energy contribution

$$\frac{F_1}{k_B T} = \sum_{i=1}^{2} \bar{\Omega}_{ci} \left[\left(1 - \frac{M_i}{\bar{\Omega}_{ci}}\right) \log\left(1 - \frac{M_i}{\bar{\Omega}_{ci}}\right) + \frac{M_i}{\bar{\Omega}_{ci}} \log\left(\frac{M_i}{\bar{\Omega}_{ci}}\right) \right], \qquad \text{eq.29}$$

where the rescaled dimensionless volume of the cylinder is $\bar{\Omega}_{ci} = (N_i - n_i)\left(\pi \tilde{d}_c{}^2 - 1/4\right)/\tilde{r}_c^3$, and $\tilde{r}_c$ and $\tilde{d}_c$ are the rescaled dimensionless ionic size parameter and the rescaled dimensionless diameter of the cylinder, respectively, given by $\tilde{r}_c = r_c/\ell$ and $\tilde{d}_c = d_c/\ell$.

Considering $N_i f_{mi} - M_i + n_s$ free ions of species i, the free energy contribution from the translational entropy of ions free in solution takes the form

$$\frac{F_2}{k_B T} = \sum_{i=1}^{2} N_i \left[\left\{ \left(f_{mi} - \frac{n}{N_i}\right)(1 - \alpha_i) + \frac{n}{N_i} + \frac{\bar{c}_s}{\bar{\rho}_i} \right\} \log\left(\bar{\rho}_i \left(f_{mi} - \frac{n}{N_i}\right)(1 - \alpha_i) + \frac{\bar{\rho}_i n}{N_i} + \bar{c}_s \right) \right. \qquad \text{eq.30}$$
$$\left. - \left\{ \left(f_{mi} - \frac{n}{N_i}\right)(1 - \alpha_i) + \frac{n}{N_i} + \frac{\bar{c}_s}{\bar{\rho}_i} \right\} \right],$$

where $\bar{\rho}_i = N_i/(\Omega/r_c^3)$ and $\bar{c}_s = n_s/(\Omega/r_c^3)$.

The free-energy contribution from the correlations between all dissociated counterions is given by

$$\frac{F_3}{k_B T} = -\Lambda \frac{\tilde{\kappa}^3 \tilde{r}_c^3}{12\pi} \frac{N_i}{\bar{\rho}_i}, \qquad \text{eq.31}$$

where the Λ is an empirical correction parameter[32] (see the following subsection for details), and the inverse Debye length, κ, is defined as

$$\tilde{\kappa}^2 = 4\pi \frac{\tilde{\ell}_B}{\tilde{r}_c^3}\left[\sum_{i=1}^{2} \bar{\rho}_i \left(f_{mi} - \frac{n}{N_i}\right)(1-\alpha_i) + \frac{\bar{\rho}_i n}{N_i} + \bar{c}_s\right], \qquad \text{eq.32}$$

with $\tilde{\kappa} = \kappa\ell$.

Including all ion pairs (monomer-counterion and oppositely charged monomers) for the complexed and the uncomplexed chain parts, the electrostatic free energy of these ion pairs is

$$\frac{F_4}{k_B T} = -\sum_{i=1}^{2} \tilde{\ell}_B \delta_i N_i \left\{\left(f_{mi} - \frac{n}{N_i}\right) - \left(1 - \frac{n_i}{N_i}\right)\right\} - n\tilde{\ell}_B \delta_{12}, \qquad \text{eq.33}$$

where $\delta_i = (\epsilon\ell/\epsilon_{li} d_{mc})$ are the dielectric 'mismatch' parameters for monomer-counterion pairing in the uncomplexed chain parts, d_{mc} is the dipole length of monomer-counterion pair, $\delta_{12} = \epsilon\ell/\epsilon_{l12} d_{mm}$ is the corresponding parameter for monomer-monomer pairing in the complexed part, and d_{mm} is the dipole length of monomer-monomer pairs. δ_i is a mean field parameter that accounts for microscopic aspects of ion pairing, and is thus simultaneously influenced by the difference between the local dielectric constants, ϵ_{li}, and the bulk dielectric constant of the medium, ϵ, as well as the effective dipole length for ion pairing. It should, however, be noted that the theory cannot provide separate estimates of the underlying microscopic parameters, i.e., the local dielectric constant and the effective dipole length.

The configurational and interaction free energy for two complexing polyions, originating from the Edwards-Muthukumar Hamiltonian[27-29], is variationally extremized[26]. The Hamiltonian is based upon an effective expansion factor ℓ_{1i} for R_{ei} of chain i with $R_{ei}^2 = N_i \ell \ell_{1i} \equiv N\ell^2 \tilde{\ell}_{1\mathrm{i}} = 6\tilde{R}_{g\mathrm{i}}^2 \ell^2$, with $\tilde{\ell}_{1\mathrm{i}} (= \ell_{1i}/\ell)$ and $\tilde{R}_{g\mathrm{i}} = \frac{R_{gi}}{\ell}$ (R_{gi} is the radius of gyration of chain *i*) being the rescaled expansion factor and radius of gyration of chain *i*, respectively. Finally, using a Gaussian monomer distribution[26,33], the free-energy contribution due to the elastic entropy, self-interaction (both electrostatic and non-electrostatic) of the individual polyions, and the mutual interaction (both electrostatic and non-electrostatic) between the polyions is obtained as

$$\begin{aligned}\frac{F_5}{k_B T} = \; & \frac{3}{2}\sum_{i=1}^{2}\left(\tilde{\ell}_{1i} - 1 - \log \tilde{\ell}_{1i}\right) + \left(\frac{9}{2\pi}\right)^{3/2} \sum_{i=1}^{2} \frac{w_{ii} N_i^{1/2}}{\tilde{\ell}_{1i}^{3/2}} + w_{12} N_1 N_2 \left(\frac{3}{4\pi \tilde{R}_{g0}^2}\right)^{3/2} \exp\left(-\frac{3\tilde{R}^2}{4\tilde{R}_{g0}^2}\right) \\ & + \sum_{i=1}^{2} \frac{f_i^2 (N_i - n_i)^2 \tilde{\ell}_B}{2} \Theta_s(\tilde{\kappa}, a_i) - f_1 f_2 (N_1 - n_1)(N_2 - n_2)\tilde{\ell}_B \Theta_m\left(\tilde{\kappa}, \tilde{R}, a_{12}\right), \end{aligned} \qquad \text{eq.34}$$

where w_{ii} and w_{12} are the self- and inter-chain two-body non-electrostatic (excluded volume) interaction strengths, respectively, $\tilde{R} = |\boldsymbol{r_1} - \boldsymbol{r_2}|/\ell = \tilde{R}_{g1} + \tilde{R}_{g2}, \tilde{R}_{g0}^2 = \sum_{i=1}^{2} \tilde{R}_{gi}^2$, with $\boldsymbol{r_1}$ and $\boldsymbol{r_2}$ being the centers of mass of the two chains, and

$$\Theta_s(\tilde{\kappa}, a_i) = \frac{2}{\pi}\left[\sqrt{\frac{\pi\tilde{\kappa}^2}{4a_i}} - \frac{\tilde{\kappa}\pi}{2} \exp(a_i)\, \mathrm{erfc}\left(\sqrt{a_i}\right)\right], \qquad \text{eq.35}$$

where $a_i = \tilde{\kappa}^2 \tilde{R}_{gi}^2 (N_i - n_i)/3N_i$, and $\Theta_m\left(\tilde{\kappa}, \tilde{R}, a_{12}\right)$ is

$$\Theta_m\left(\tilde{\kappa}, \tilde{R}, a_{12}\right) = \frac{e^{a_{12}}}{\tilde{R}}\left[e^{-\tilde{\kappa}\tilde{R}}\, \mathrm{erfc}\left(\sqrt{a_{12}} - \frac{\tilde{\kappa}\tilde{R}}{2\sqrt{a_{12}}}\right) - e^{\tilde{\kappa}\tilde{R}}\, \mathrm{erfc}\left(\sqrt{a_{12}} + \frac{\tilde{\kappa}\tilde{R}}{2\sqrt{a_{12}}}\right)\right], \qquad \text{eq.36}$$

where $a_{12} = \sum_{i=1}^{2} \tilde{\kappa}^2 \tilde{R}_{gi}^2 (N_i - n_i)/6N_i$.

Due to the differences in size and/or charge density of the chains, the total free energy, $F_1 + F_2 + F_3 + F_4 + F_5$ (eqs. 29-31 & 33-34), is minimized with respect to four variables, f_{T1}, f_{T2}, $\tilde{\ell}_{11}$, and $\tilde{\ell}_{12}$, using the Nelder-Mead simplex algorithm, using four adjustable parameters δ_0 $(= \delta_1 = \delta_2)$, δ_{12}, w_0 $(= w_1 = w_2 = w_{12})$, and Λ, while r_c is fixed (see the section on parameterization). The free energy was originally constructed[26] for generic values of the overlap parameter n, and ideally, the dangling and complexed parts of each polyion had to be considered as two different chains with different size scaling (given by a single size expansion factor ℓ_1). In the present problem, however, only configurations of fully isolated $(n = 0)$ and fully complexed $(n = N_{c1})$ polyions are of interest, for which the entire polyion can be assumed to have the same size scaling.

Free energy of a single partially ionized flexible polyelectrolyte

We use measurements of ProTα and H1 in isolation for defining the single-chain parameters of the theory[26,29] (see below) and thus also require the expression for the free energy of a single, isolated polyelectrolyte chain. The parameters for the various free energy components, F_1 to F_5, are analogous to the ones for two-chain complexation, and the single-chain expression can be obtained from eqs. 29-31 & 33-34 by setting $n = 0$, choosing the expression for one of the chains (removing the index *i*), and removing terms involving mutual interaction between the polyions ($\delta_{12}, w_{12}, f_1 f_2$ terms):

$$\frac{F_1}{k_B T} = \bar{\Omega}_c \left[\left(1 - \frac{M}{\bar{\Omega}_c}\right) \log\left(1 - \frac{M}{\bar{\Omega}_c}\right) + \left(\frac{M}{\bar{\Omega}_c}\right) \log\left(\frac{M}{\bar{\Omega}_c}\right) \right], \qquad \text{eq.37}$$

where $\bar{\Omega}_c = \frac{N}{\tilde{r}_c^3}\left(\pi \tilde{d}_c{}^2 - 1/4\right)$.

$$\frac{F_2}{k_B T} = N\left\{ (f\bar{\rho} + \bar{c}_s) \log\left(f + \frac{\bar{c}_s}{\bar{\rho}}\right) + \frac{\bar{c}_s}{\bar{\rho}} \log \bar{c}_s - (f\bar{\rho} + \bar{c}_s) \right\} \qquad \text{eq.38}$$

$$\frac{F_3}{k_B T} = -\Lambda \frac{\Omega \kappa^3}{12\pi} = -\Lambda \frac{N\sqrt{4\pi\tilde{\ell}_B}^{\,3/2}}{3\bar{\rho}} (f\bar{\rho} + \bar{c_s})^{3/2} = -\Lambda \frac{(\tilde{\kappa}\tilde{r}_c)^3}{12\pi}, \qquad \text{eq.39}$$

where $\tilde{\kappa} = \sqrt{\frac{4\pi\tilde{\ell}_B}{\tilde{r}_c^3}(\bar{\rho}f + \bar{c_s})}$.

$$\frac{F_4}{k_B T} = -(1-f) N \delta \tilde{\ell_B} \qquad \text{eq.40}$$

As before, N is the number of monomers in the chain, f the degree of ionization, $\bar{\rho}$ the rescaled monomer density, $\bar{c}_s$ the rescaled salt concentration, and κ the inverse Debye length. The dielectric mismatch parameter is $\delta = (\epsilon\ell/\epsilon_l d)$, with ϵ_l being the local dielectric constant, and d the dipole length of monomer-counter ion pairs. The configurational free energy of the chain is obtained by the variational method[26,28], in which one starts from the Edwards-Muthukumar Hamiltonian, considering uniform swelling of the chain with spherical symmetry,

$$\frac{F_5}{k_B T} = \frac{3}{2}\left[\tilde{\ell}_1 - 1 - \log \tilde{\ell}_1\right] + \left(\frac{9}{2\pi}\right)^{3/2} w\sqrt{N}\,\frac{1}{\tilde{\ell}_1^{3/2}} + 2\sqrt{\frac{6}{\pi}} f^2 \tilde{\ell}_B \frac{N^{3/2}}{\tilde{\ell}_1^{1/2}} \Theta_0(\tilde{\kappa}, a), \qquad \text{eq.41}$$

where $\tilde{\ell}_1$ is the size expansion factor of the chain, and

$$\Theta_0(\tilde{\kappa}, a) = \frac{2}{\pi}\left[\sqrt{\frac{\pi\tilde{\kappa}^2}{4\,\mathrm{a}}} - \frac{\tilde{\kappa}\pi}{2}\exp(a)\,\mathrm{erfc}\left(\sqrt{a}\right)\right], \qquad \text{eq.42}$$

with $a \equiv \tilde{\kappa}^2 N \tilde{\ell}_1/6$, where a Gaussian monomer distribution for the chain has been used[26,33].

Correction for the electrostatic free energy contribution due to the correlations between free ions at high salt concentrations

The bare Debye-Hückel term in F_3 (eqs. 31 & 39) is insufficient for quantitatively describing the free energy at high salt concentrations (for $\kappa^{-1} \leq \ell_B$), so we invoke the empirical parameter Λ as a correction factor to obtain reasonable agreement with the experimental observables[32]. To this end, we turn to the starting point of the Debye-Hückel formalism, which is based on solving the Poisson-Boltzmann (PB) equation for the charge density of the ionic species in solution and the necessary approximation of linearizing the PB equation for low salt concentration, hence for small κ. This approach leads to $F_3/k_BT \simeq -\Omega\kappa^3/12\pi$.[34] At high salt, the linearization of the PB equation breaks down, and furthermore, the ionic atmosphere moving around the ion remains no longer symmetrical with respect to the charge distribution of the surrounding ions. These effects modify the electrostatic screening length and lead to multiple screening lengths distinct from that of the usual uniform Debye screening length κ^{-1}.[32]

Due to the presence of multiple electrostatic decay lengths, the modified mean electrostatic potential experienced by an ion q_j, $\psi_i^{\text{high}}(r)$, at high salt can be written as a perturbation sum over all possible decay lengths, of the form

$$\begin{aligned}\psi_i^{\text{high}}(r) \quad &= \frac{q_i^{\text{eff}_1}}{4\pi\epsilon_r^{\text{eff}_1}\epsilon_0}\frac{e^{-\kappa_1 r}}{r} + \frac{q_i^{\text{eff}_2}}{4\pi\epsilon_r^{\text{eff}_2}\epsilon_0}\frac{e^{-\kappa_2 r}}{r} + \cdots \\ &\simeq \frac{\Lambda q_i^{\text{eff}}}{4\pi\epsilon_r\epsilon_0}\frac{e^{-\kappa r}}{r} \\ &= \Lambda\psi_i(r)\,,\end{aligned} \qquad \text{eq.43}$$

where κ_1, κ_2, etc. are the electrostatic decay lengths, and $q_i^{\text{eff}_1}$, $q_i^{\text{eff}_2}$, etc. are the effective charges as experienced by q_j, and $\epsilon_r^{\text{eff}_1}$, $\epsilon_r^{\text{eff}_2}$ represent the effective dielectric permittivity values (different from the solvent permittivity, ϵ_r) in the non-uniform ionic atmosphere. The effect of asymmetry in the charge distribution and the associated change in dielectric permittivity is collapsed into a single correction factor, Λ, with the potential form being kept invariant with respect to the bare Debye-Hückel term with a single decay length. Λ remains a multiplicative scalar upon integrating $\psi_i(r)$ to obtain the total electrostatic potential, and hence the free energy (eqs. 31 & 39)[34]. Ideally, Λ should be salt concentration-dependent; however, given that we apply the theory at moderately high salt concentrations across a relatively narrow concentration range, Λ was treated as a salt-invariant fit parameter for both the single-chain dimensions and the components of the free energy of complexation, and chosen by optimizing the agreement of the theory with the salt dependence of the free energy of chain complexation observed experimentally. Λ introduces minor modifications to the enthalpy of complexation (see Fig. S3B), whereas the major contribution comes from the entropy of the condensed and released ions and from the electrostatic free energy of condensed ions.

We estimate a release of ~45-60 counterions from the theory (depending on salt concentration), as opposed to ~18 estimated from the salt-dependent free energy of chain complexation using the Record-Lohmann framework[2,16]. Accounting for salt concentration-dependent ionic correlations significantly alters the entropy and enthalpy of counterion adsorption and release and consequently the thermodynamics of chain complexation; specifically, the number of counterions released is salt concentration-dependent. These aspects are not considered in the Record-Lohman framework and are the likely origin of the difference in estimates of counterion release from the two approaches. In other words, a larger number of counterions can actually be released upon chain complexation than would be

suggested from a Record-Lohman analysis of the salt dependence of the free energy or entropy.

Parameterization of the system and numerical optimization of the parameters

Upon eliminating the excluded volume and screened Coulomb interaction terms from the free energy of a single, isolated polyion, one recovers the theta-state dimensions of the chain given by $R_e = \sqrt{N}l$, where N and l are the number of segments and the segment length, respectively. The $C_\alpha - C_\alpha$ distance is 0.38 nm, but the theta-state dimensions for generic IDPs have been observed to be well approximated by $R_e = 0.55\ \mathrm{nm}\sqrt{N}$;[10,35] the increase in the effective segment length for the theta state from 0.38 nm to 0.55 nm is likely to be caused by local chain stiffness[36]. However, the contour length, L, is given by $0.38\ \mathrm{nm}\,N$, and thus using 0.55 nm as a segment length would result in physically unrealistic chain dimensions. We thus rescale both N and l to obtain the rescaled parameters N' and l' by solving $N'l' = 0.38\ \mathrm{nm}\,N$ and $\sqrt{N'}l' = 0.55\ \mathrm{nm}\sqrt{N}$, which yields l' = 0.8 nm and $N' = 0.48N$. With the rescaled parameters, we essentially obtain a projection of a generic IDP theta state on a Gaussian chain and recover both the theta state and the contour length. For ProTα, N' is 53. For H1, we approximated the contour as a 130-residue long IDP by replacing the folded domain with an effective chain segment of 10 peptide bonds (10 peptide bonds with a length scaling exponent of 0.63, representative of an expanded chain, matches the $C_\alpha - C_\alpha$ distance between the first and last structurally resolved residues of the globular domain; note that the exact choice of the scaling exponent minimally affects the length of the chain segment replacing the folded domain). This approach renders H1 amenable to investigation with our theory and is unlikely to strongly affect the interpretation, given that the globular domain contributes minimally to the overall dimensions, net-charge and binding affinity of H1 for ProTα[2]. The resulting value of N' we used for H1 is 62. For further parameterization, we used the measured chain dimensions of ProTα as described above, and for the same salt concentrations, the H1 chain dimensions were approximated by those of a chain with the same length scaling exponent experimentally obtained for ProTα and 129 peptide bonds.

The strength of the excluded volume interaction of the individual chains, w, can be obtained from the experimental single-chain dimensions at high salt concentration (Fig. S1) based on the configurational free energy of a single polyelectrolyte chain (eq. 41). With vanishing charge interactions (since at high salt concentrations, electrostatic interactions are effectively screened), the effective free energy at high salt takes the form:

$$\frac{F_5}{k_B T} = \frac{3}{2}\left[\tilde{\ell}_1 - 1 - \log\tilde{\ell}_1\right] + \left(\frac{9}{2\pi}\right)^{3/2} w\sqrt{N}\frac{1}{\tilde{\ell}_1^{3/2}}, \qquad \text{eq.44}$$

which upon minimization leads to a crossover relation for the chain expansion factor, $\tilde{\ell}_1$, as a function of w,

$$\tilde{\ell}_1^{5/2} - \tilde{\ell}_1^{3/2} = \left(\frac{9}{2\pi}\right)^{3/2} w\sqrt{N}, \qquad \text{eq.45}$$

which can be used to obtain the initial estimates for w to match the theoretical R_e of the chain with the experimentally obtained R_e at high salt concentration.

The rescaled ion size parameter, $\tilde{r}_c$, was set to 0.3; in terms of single-chain dimensions, for a given value of δ, the exact value of $\tilde{r}_c$ is virtually inconsequential within the range $1 \geq \tilde{r}_c > 0$, that is, for ion sizes smaller than the monomer length. In view of the low sensitivity of the result to variations in the excluded-volume parameters for ProTα-H1 complexation — which may not be surprising given the dominance of electrostatic interactions in such a highly charged system — we used a single excluded volume parameter, w_0 ($w_0 =$

$w_1 = w_2 = w_{12}$), for all non-electrostatic inter- and intra-chain interactions, and we estimated its value based on the dimensions of ProTα and H1 at high salt concentrations (above ~0.5 M; Fig. S4C) using eq. (45). We also used a single dielectric mismatch value δ_0 ($\delta_0 = \delta_1 = \delta_2$) for chain-counterion interactions, and we estimated bounds on δ_0 from the chain dimensions of ProTα and H1 and its experimental uncertainty at the lowest salt concentration using eqs. (37-41) and setting w_0 to the value obtained in the first step. In the next step, with w_0 fixed from the value obtained in the first step and δ_0 constrained to the bounds estimated form the previous step, we obtained values for δ_0, δ_{12}, and Λ by minimizing, based on a grid search, the residual sum of squares between experimental and computed free energy and enthalpy values associated with chain complexation, as a function of salt concentration using eqs. (29-34). To account for the different number of data points from chain complexation enthalpy (calorimetry) and chain complexation free energy (single-molecule FRET), the residual sums of squares were divided by the respective number of data points in the minimization. With the resulting parameter values, both the thermodynamic data (Fig. 4G) and the chain dimensions (Fig. 4F) as a function of salt concentration are described well by the theory.

Assessing the potential effect of charge regulation

To obtain an estimate of the contribution of charge regulation, we used the approach developed by Mulder and co-workers for unfolded and disordered proteins[37], building on site-specific information on protonation equilibria from NMR[38] and implemented in the pepKalc server[37]. Calculations for the ProTα sequence with pepKalc indicate that the structural charge (the charge at a given pH assuming unshifted canonical pK_a values for ionizable sidechains) of ProTα is recovered above ~100 mM salt (see Fig. S4). Furthermore, pH-dependent NMR experiments of the highly acidic C-terminal tubulin tail (NCPR of 0.34 vs. 0.40 for ProTα) also indicate that the net charge at neutral pH equals the structural charge in the presence of ~100 mM NaCl[39], in agreement with the pepKalc results on this protein. These results suggest that at salt concentrations where we measure H1-ProTα heterodimer formation, the salt concentration is high enough to suppress charge regulation. However, at low salt concentrations, the effect is significant and is therefore likely to affect our estimates of chain dimensions. To test this aspect, we estimated the chain dimensions for ProTα using eqs. 37-41 with the values of w_0 and δ_0 from Table S5, but setting the charge of ProTα to the value estimated from pepKalc at each salt concentration. The difference in dimensions using a nominal charge of -44 and using the charges from pepKalc is small compared to the relatively large experimental error (owing to the low transfer efficiencies observed in this range, Fig. S4). We note that this is an approximate approach; more precise effects of charge regulation would require a self-consistent theoretical framework including counterion condensation, charge regulation, and chain dimensions.

SI Figures and Tables

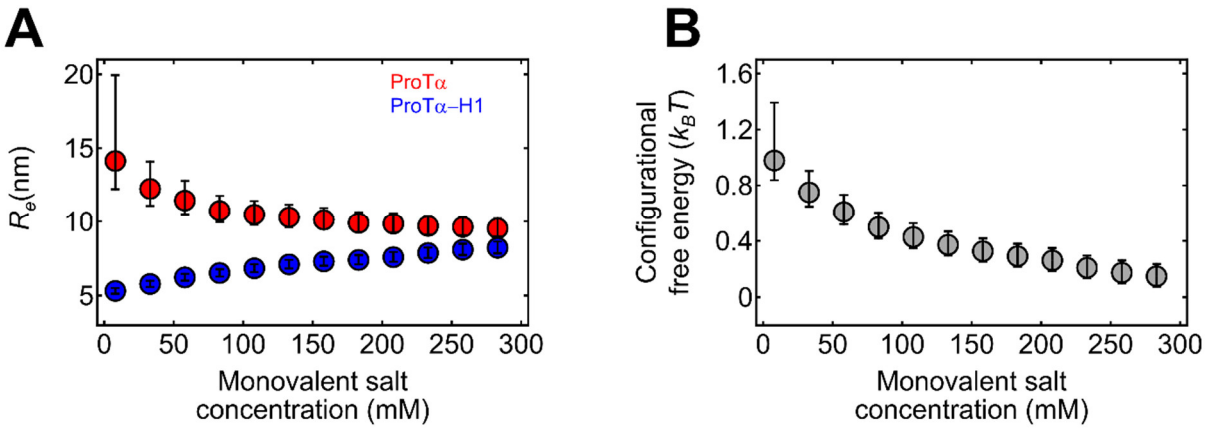

Figure S1: (A) R_e for unbound (red) and H1-bound (blue) ProTα as a function of monovalent salt concentration measured using single-molecule FRET with 2C/110C ProTα (in 10 mM Tris buffer, monovalent salt concentration adjusted with KCl). The error bars are estimated from a conservative systematic error ±0.03 on transfer efficiencies. (B) Configurational free energy change of ProTα upon H1 binding estimated from the change in R_e (A) using eq. 9. The error bars represent the error propagated from the errors on R_e (A). Note that the total change in configurational free energy upon binding (for both chains) does not exceed 2 k_BT even in the absence of added salt, where the compaction is maximal.

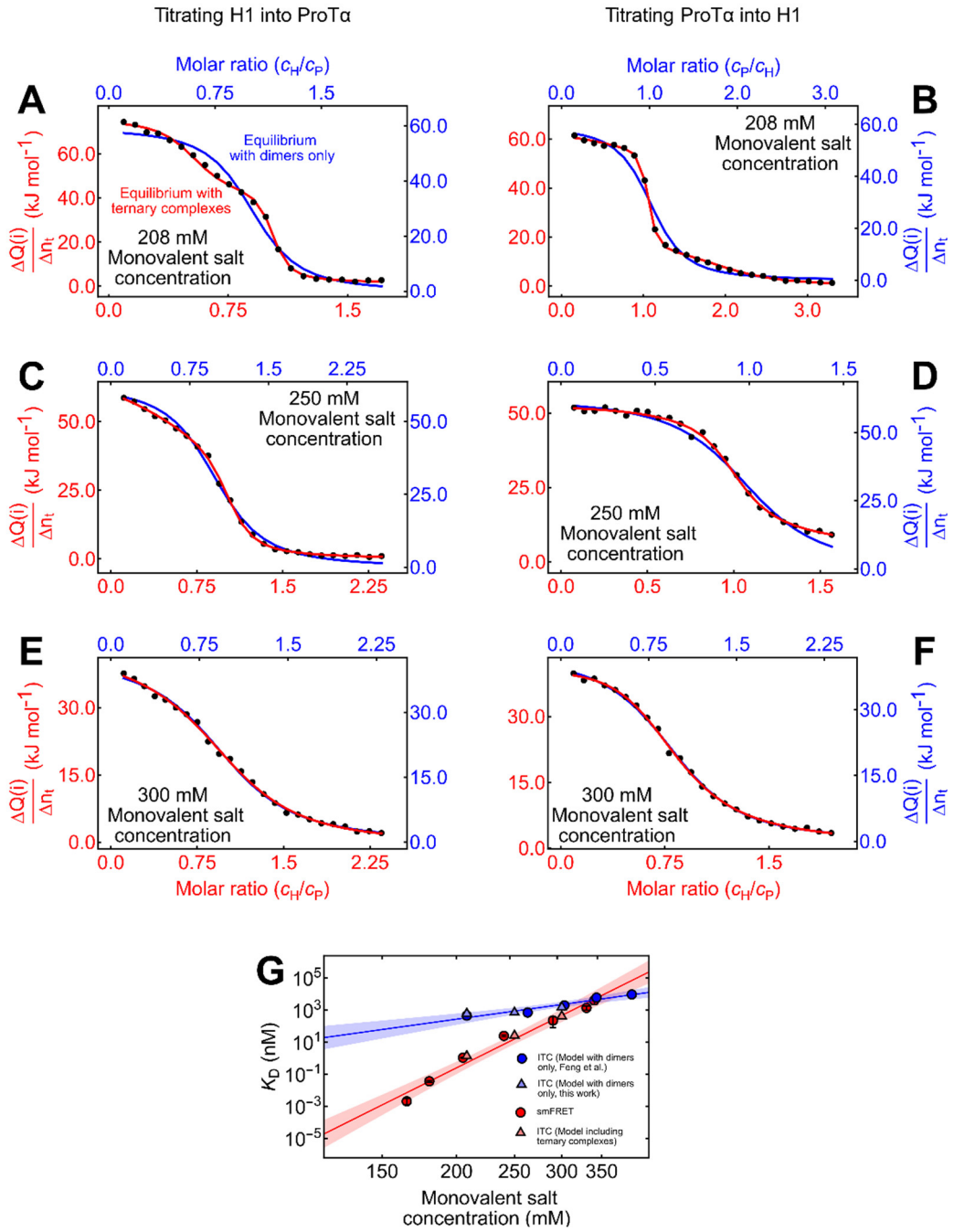

Figure S2: (A-F) Integrated power from ITC per molar amount of injected titrant ($\Delta Q/\Delta n_t$; black points for each injection *i*) as a function of molar ratio the two proteins upon titrating H1 into ProTα (A, C & E) and titrating ProTα into H1 (B, D & F) at monovalent salt concentrations of 208 mM (A,B), 250 mM (C,D), and 300 mM (E,F). The data in (A-F) are globally fitted either with a 1:1 binding model (blue line and blue axis labels), or with a model including PHH and PPH ternary complexes (red line and axis labels). Note that the molar ratio is a fit parameter and thus slightly different for the two analyses (top and bottom axes). (G) Comparison of the dissociation constants for heterodimer formation from single-molecule FRET and ITC. Circles show K_D^{PH} from single-molecule FRET (red, data and errors from Borgia et al.[2]) and apparent dissociation constants from ITC analyzed with a 2-state model (blue, from Feng et al.[40]). Triangles represent apparent dissociation constants from ITC (A-F) using a 2-state model (blue) or the model including ternary complex formation (red). Solid lines represent fits with Eq. 3 (Main text) and shaded bands the corresponding 90% confidence intervals.

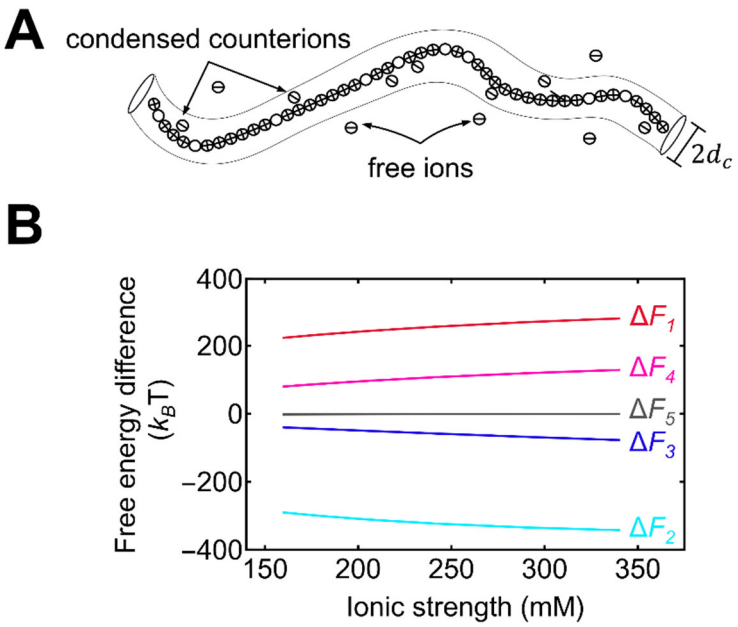

Figure S3: (A) Schematic of the cylindrical volume around the polyions that is used for calculating the local counterion condensation entropy. The radius of the cylinder is taken to be d_c (see text for definition). All counterions inside the cylinder are considered to be condensed to the chain but free to move within the cylinder. (B) Dependence of the differences in the free energy components between uncomplexed and fully complexed chains (components of the free energy of chain complexation), ΔF_1 (entropy of condensed ions), ΔF_2 (entropy of free ions), ΔF_3 (correlation of dissociated ions), ΔF_4 (Coulomb free energy of ion-pair formation), and ΔF_5 (conformational free energy of the chains) on salt concentration, computed using the parameters in Table S5.

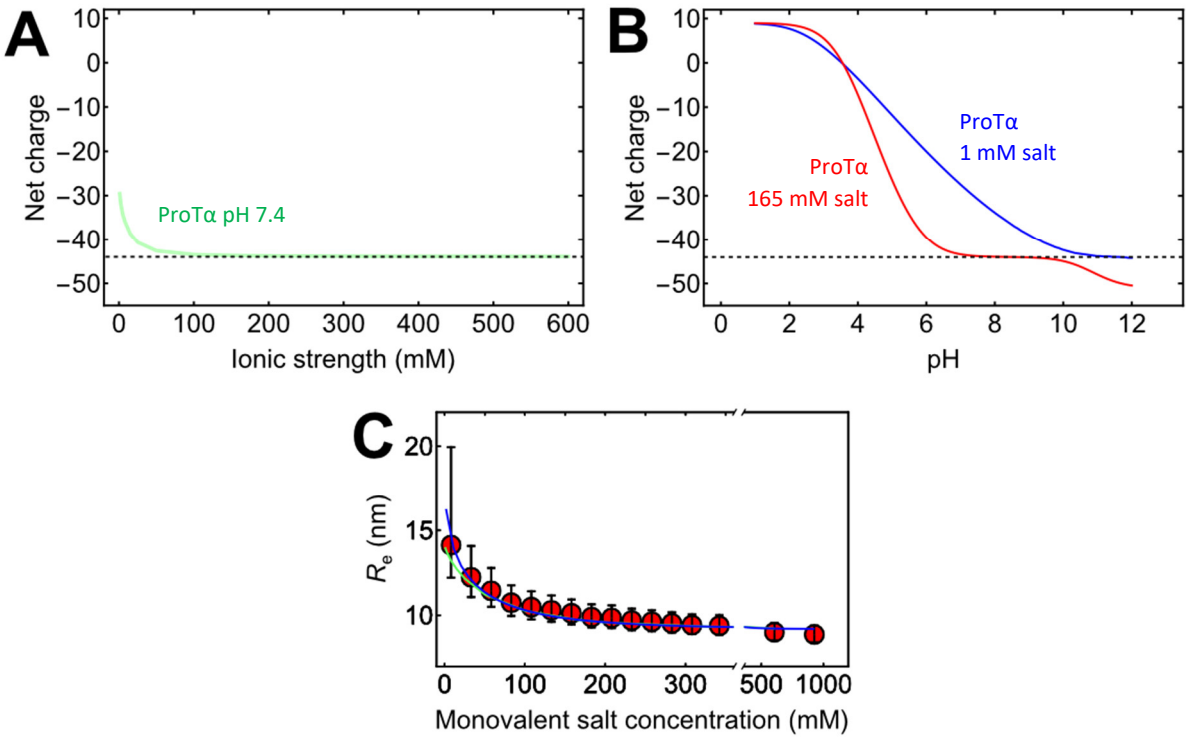

Figure S4: (A, B) Calculations of the salt concentration-dependent net charge of ProTα performed using the pepKalc server (https://st-protein02.chem.au.dk/pepkalc/). (A) Net charge of ProTα at pH 7.4 as a function of ionic strength. The dashed black lines indicate the structural charge based on the tabulated pK_a values of the acidic and basic groups of the free amino acids at pH 7.4. (B) Net charge of ProTα as a function of pH at 1 mM ionic strength (blue curve) and 165 mM ionic strength (red curve). Similar calculations for H1 also indicate recovery of its structural charge at ~100 mM ionic strength. (C) R_e for unbound ProTα as a function of monovalent salt concentration measured using single-molecule FRET with 2C/110C ProTα (filled circles). The error bars are estimated from a conservative systematic uncertainty of ±0.03 on transfer efficiencies. The blue line represents R_e using the theory for a single, isolated polyelectrolyte chain (as in Fig. 4F) using a net charge of -44; the green line represents estimates from the theory where the charge of ProTα was set to the ionic strength-dependent values shown in (A). All parameters except the charge are kept at the values given in Table S5.

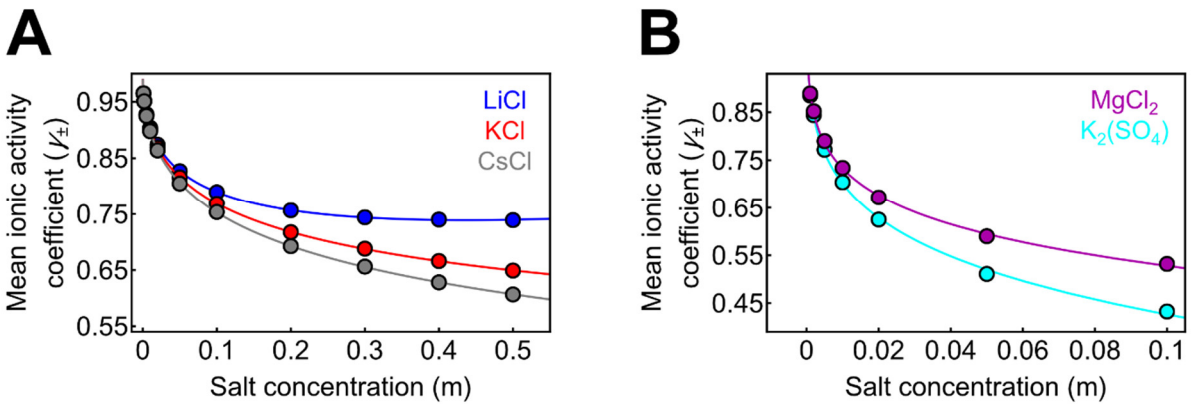

Figure S5: (A) Mean ionic activity coefficients, $\gamma_\pm$, as a function of molal concentration of monovalent salts, *m*, for KCl (red), LiCl (Blue) and CsCl (gray) [12] interpolated with the empirical functions given in Table S4 (lines). **(B)** $\gamma_\pm$ as a function of molal concentration of salts with a divalent cation or divalent anion, $MgCl_2$ (magenta) and $K_2(SO_4)$ (cyan), respectively [12], interpolated with the empirical functions given in Table S4 (lines).

Monovalent salt concentration (mM)	Titrant	Apparent K_D (μM)	Apparent ΔH $\left(\frac{kJ}{mol}\right)$	% Deviation from nominal titrant concentration	% Deviation from nominal titrand concentration	χ^2
208	ProTα	0.8	59.0	+19.8	-5.2	9.71
208	H1	0.8	59.0	+18.6	+8.9	9.44
250	ProTα	0.9	62.3	-0.9	0.0	5.89
250	H1	0.9	62.3	+20	0.0	3.89
300	ProTα	1.9	42.7	+19.0	-18.4	0.35
300	H1	1.9	42.7	-2.2	-7.2	0.51

Table S1: Parameters obtained from a global fit of the ITC data imposing a 2-state model. Note that we use titrant and titrand concentrations as fit parameters instead of stoichiometry (see Methods).

Monovalent salt concentration (mM)	Titrant	$K_{D(1)}^{PH}$ (nM)	$K_{D(2)}^{PH}$ (nM)	$\lvert\Delta G_{(1)}^{PH} - \Delta G_{(2)}^{PH}\rvert$ (k_BT)	$K_{D(1)}^{PPH}$ (μM)	$K_{D(2)}^{PPH}$ (μM)	$\lvert\Delta G_{(1)}^{PPH} - \Delta G_{(2)}^{PPH}\rvert$ (k_BT)	$K_{D(1)}^{PHH}$ (μM)	$K_{D(2)}^{PHH}$ (μM)	$\lvert\Delta G_{(1)}^{PHH} - \Delta G_{(2)}^{PHH}\rvert$ (k_BT)	ΔH^{PH} $\left(\frac{kJ}{mol}\right)$	ΔH^{PPH} $\left(\frac{kJ}{mol}\right)$	ΔH^{PHH} $\left(\frac{kJ}{mol}\right)$	Deviation from nominal titrant concentration (%)	Deviation from nominal titrand concentration (%)	χ^2
208	ProTα	1.7	0.5	1.2	2.6	3.3	0.2	8.9	14	0.5	58.2	17.6	4.2	+12.9	-16.3	0.38
208	H1	1.7	0.5	1.2	2.6	3.3	0.2	8.9	14	0.5	58.2	17.6	4.2	-5.3	-2.3	0.88
250	ProTα	32	16	0.7	15	14	0.1	7.0	18	0.9	49.8	19.7	2.5	+8.9	+20.0	1.02
250	H1	32	16	0.7	15	14	0.1	7.0	18	0.9	49.8	19.7	2.5	+13.0	-9.4	0.49
300	ProTα	51	470	0.1	150	58	1.0	8.5	23	0.9	36.8	15.9	3.8	+19.0	-10.4	0.28
300	H1	51	470	0.1	150	58	1.0	8.5	23	0.9	36.8	15.9	3.8	-6.7	-2.6	0.39

Table S2: Parameters obtained by globally fitting the ITC data with the complete model including ternary complex formation. $K_{D(1)}^{X}$ and $\Delta G_{(1)}^{X}$ represent values from ITC, and $K_{D(2)}^{X}$ and $\Delta G_{(2)}^{X}$ correspond to values from the extrapolation of salt-dependent dissociation constants (Fig. 4a and Fig. S2). Note that we use titrant and titrand concentrations as fit parameters instead of stoichiometry (see Methods).

Unlabeled ProTα (WT isoform 2)	GPMSDAAVDTSSEITTKDLKEKKEVVEEAENGRDAPANGNANEENGE QEADNEVDEEEEEGGEEEEEEEEGDGEEEDGDEDEEAESATGKRAAE DDEDDDVDTKKQKTDEDD
Labeled ProTα 2C/110C (isoform 1)	GP**C**DAAVDTSSEITTKDLKEKKEVVEEAENGRDAPANGNAENEENGEQ EADNEVDEEEEEGGEEEEEEEEGDGEEEDGDEDEEAESATGKRAAED DEDDDVDTKKQKTDED**C**
Labeled ProTα 2C/110C (isoform 1)	G**C**DAAVDTSSEITTKDLKEKKEVVEEAENGRDAPANGNAENEENGEQE ADNEVDEEEEEGGEEEEEEEEGDGEEEDGDEDEEAESATGKRAAEDD EDDDVDTKKQKTDED**C**GA
Labeled ProTα 56C/110C (isoform 1)	GPSDAAVDTSSEITTKDLKEKKEVVEEAENGRDAPANGNAENEENGEQ EADNEVDEE**C**EEGGEEEEEEEEGDGEEEDGDEDEEAESATGKRAAED DEDDDVDTKKQKTDED**B**
Unlabeled H1	TENSTSAPAAKPKRAKASKKSTDHPKYSDMIVAAIQAEKNRAGSSRQSI QKYIKSHYKVGENADSQIKLSIKRLVTTGVLKQTKGVGASGSFRLAKSD EPKKSVAFKKTKKEIKKVATPKKASKPKKAASKAPTKKPKATPVKKAKK KLAATPKKAKKPKTVKAKPVKASKPKKAKPVKPKAKSSAKRAGKKK

Table S3: Amino acid sequences of the proteins used. Cysteine residues introduced for fluorophore conjugation are highlighted in red. All labeled variants are ProTα isoform 1, while unlabeled ProTα is isoform 2; the isoforms differ by a single glutamate residue at position 39[1]. The two variants of labeled ProTα 2C/110C originate from different expression constructs, but the cysteine positions and the intervening sequences are identical, resulting in experimentally indistinguishable behavior.

Salt	Fit equation	Fit parameters		
		A	B	C
KCl	$\gamma_{\pm} = 10^{\left[\frac{-0.5108\sqrt{\left(\frac{m}{mol\,kg^{-1}}\right)}}{1+B\sqrt{\left(\frac{m}{mol\ kg^{-1}}\right)}}+C\left(\frac{m}{mol\,kg^{-1}}\right)\right]}$	-	1.3198	-0.0014
LiCl		-	1.3440	0.1084
CsCl		-	1.0369	-0.0171
$MgCl_2$	$\gamma_{\pm} = A + C\left(\frac{m}{mol\,kg^{-1}}\right)^{B}$	1.4731	0.1061	-1.2068
$K_2(SO_4)$		1.3084	0.1623	-1.2818

Table S4: Empirical equations used for fitting mean ionic activity coefficient ($\gamma_{\pm}$) as a function of molal concentration of salts (m), for different salts (Fig. S6), with the resulting fit parameters.

Parameter	Value	Parameter fixed or adjustable	Physical significance of the parameter
N_1	53	Fixed (See discussion on parameterization)	Number of Kuhn segments in the polyelectrolyte chains; N_1 refers to ProTα and N_2 to H1.
N_2	62		
N_{c1}	44	Fixed (See discussion on parameterization)	Charges of the polyelectrolyte chain; N_{c1} refers to ProTα and N_{c2} to H1.
N_{c2}	53		
$\ell(nm)$	0.8	Fixed (See discussion on parameterization)	Length of a Kuhn segment
$\tilde{r}_c$	0.3	Fixed (See discussion on parameterization)	The diameter of the counterions divided by the Kuhn segment length. In this case, the diameter of the counterions, r_c, is 0.24 nm.
w_0	1.8	Adjustable (See discussion on parameterization)	Represents the monomer-monomer two-body interaction strengths (inter and intra-chain) and determine the excluded volume in the absence of electrostatics.
δ_0	3.85	Adjustable (See discussion on parameterization)	Represent the dielectric mismatch parameters, which are mean field parameters encompassing two physical quantities, an effective dipole length and a local dielectric constant. This mean field parameter determines the ion pair free energy. (Note that from the theory or the experiments, the local dielectric constant and the dipole length cannot be determined independently.) δ_0 is the dielectric mismatch parameter for ProTα-counterion and H1-counterion pairing, and δ_{12} is the value for ProTα-H1 ion pairing.
δ_{12}	1.8		
Λ	2.0	Adjustable (See discussion on parameterization)	This parameter acts as a multiplicative correction factor to the expression of free energy from ionic correlations using Debye-Hückel screening. It is required since pure Debye-Hückel screening underestimates the free energy from ionic correlations at high salt. See discussion on this correction factor.

Table S5: Parameters used in the theory to calculate the free energy and enthalpy of chain complexation and chain dimensions with their values, nature (free or adjustable), and physical significance.

SI References

1. A Sottini, A Borgia, MB Borgia, K Bugge, D Nettels, A Chowdhury, PO Heidarsson, F Zosel, RB Best, BB Kragelund, & B Schuler (2020) Polyelectrolyte interactions enable rapid association and dissociation in high-affinity disordered protein complexes. *Nat. Commun.* 11:5736.
2. A Borgia, MB Borgia, K Bugge, VM Kissling, PO Heidarsson, CB Fernandes, A Sottini, A Soranno, KJ Buholzer, D Nettels, BB Kragelund, RB Best, & B Schuler (2018) Extreme disorder in an ultrahigh-affinity protein complex. *Nature* 555:61-66.
3. S Müller-Späth, A Soranno, V Hirschfeld, H Hofmann, S Rüegger, L Reymond, D Nettels, & B Schuler (2010) Charge interactions can dominate the dimensions of intrinsically disordered proteins. *Proc. Natl. Acad. Sci. USA* 107:14609-14614.
4. N Galvanetto, MT Ivanović, A Chowdhury, A Sottini, MF Nüesch, D Nettels, RB Best, & B Schuler (2023) Extreme dynamics in a biomolecular condensate. *Nature* 619:876-883.
5. A Chowdhury, SA Kovalenko, IV Aramburu, PS Tan, NP Ernsting, & EA Lemke (2019) Mechanism-Dependent Modulation of Ultrafast Interfacial Water Dynamics in Intrinsically Disordered Protein Complexes. *Angew. Chem. Int. Ed.* 58:4720-4724.
6. V Kudryavtsev, M Sikor, S Kalinin, D Mokranjac, CAM Seidel, & DC Lamb (2012) Combining MFD and PIE for Accurate Single-Pair Förster Resonance Energy Transfer Measurements. *ChemPhysChem* 13:1060-1078.
7. D Nettels, S Müller-Späth, F Küster, H Hofmann, D Haenni, S Rüegger, L Reymond, A Hoffmann, J Kubelka, B Heinz, K Gast, RB Best, & B Schuler (2009) Single molecule spectroscopy of the temperature-induced collapse of unfolded proteins. *Proc. Natl. Acad. Sci. USA* 106:20740–20745.
8. T Yang, J Choo, S Stavrakis, & A de Mello (2018) Fluoropolymer-Coated PDMS Microfluidic Devices for Application in Organic Synthesis. *Chem. Eur. J.* 24:12078-12083.
9. RKP Benninger, Y Koç, O Hofmann, J Requejo-Isidro, MAA Neil, PMW French, & AJ deMello (2006) Quantitative 3D Mapping of Fluidic Temperatures within Microchannel Networks Using Fluorescence Lifetime Imaging. *Anal. Chem.* 78:2272-2278.
10. ED Holmstrom, A Holla, W Zheng, D Nettels, RB Best, & B Schuler (2018) Accurate Transfer Efficiencies, Distance Distributions, and Ensembles of Unfolded and Intrinsically Disordered Proteins From Single-Molecule FRET. *Methods Enzymol.* 611:287-325.
11. K Gast, H Damaschun, K Eckert, K Schulze-Forster, HR Maurer, M Mueller-Frohne, D Zirwer, J Czarnecki, & G Damaschun (1995) Prothymosin .alpha.: A Biologically Active Protein with Random Coil Conformation. *Biochemistry* 34:13211-13218.
12. CRC (2013) *Handbook of Chemistry and Physics* (CRC Press Inc. 2013, Boca Raton).
13. W Zheng, GH Zerze, A Borgia, J Mittal, B Schuler, & RB Best (2018) Inferring properties of disordered chains from FRET transfer efficiencies. *J. Chem. Phys.* 148.
14. M Aznauryan, L Delgado, A Soranno, D Nettels, J-r Huang, AM Labhardt, S Grzesiek, & B Schuler (2016) Comprehensive structural and dynamical view of an unfolded protein from the combination of single-molecule FRET, NMR, and SAXS. *Proc. Natl. Acad. Sci. USA* 113:E5389-E5398.
15. M Rubinstein & RH Colby (2003) *Polymer physics* (Oxford University Press, Oxford ; New York) pp xi, 440 p.
16. MT Record, Jr., CF Anderson, & TM Lohman (1978) Thermodynamic analysis of ion effects on the binding and conformational equilibria of proteins and nucleic acids: the roles of ion association or release, screening, and ion effects on water activity. *Q. Rev. Biophys.* 11:103-178.
17. T Engel & P Reid (Philip Reid) *Physical Chemistry 3rd Editio* (Pearson Education, Inc. 2012).
18. MM Garner & DC Rau (1995) Water release associated with specific binding of gal repressor. *EMBO J.* 14:1257-1263.

19. HP Lehmann, X Fuentes-Arderiu, & LF Bertello (1996) Glossary of terms in quantities and units in Clinical Chemistry (IUPAC-IFCC Recommendations 1996). *Pure Appl. Chem.* 68:957-1000.
20. J Tellinghuisen (2007) Calibration in isothermal titration calorimetry: Heat and cell volume from heat of dilution of NaCl(aq). *Anal. Biochem.* 360:47-55.
21. MicroCal (2014) *ITC200 System User Manual* (Malvern Instruments Ltd.).
22. JD Chodera & DL Mobley (2013) Entropy-Enthalpy Compensation: Role and Ramifications in Biomolecular Ligand Recognition and Design. *Annu. Rev. Biophys.* 42:121-142.
23. J Tellinghuisen & JD Chodera (2011) Systematic errors in isothermal titration calorimetry: Concentrations and baselines. *Anal. Biochem.* 414:297-299.
24. H Naghibi, A Tamura, & JM Sturtevant (1995) Significant discrepancies between van't Hoff and calorimetric enthalpies. *Proc. Natl. Acad. Sci. USA* 92:5597-5599.
25. S Mitra & A Kundagrami (2023) Polyelectrolyte complexation of two oppositely charged symmetric polymers: A minimal theory. *J. Chem. Phys.* 158:014904.
26. S Ghosh, S Mitra, & A Kundagrami (2023) Polymer complexation: Partially ionizable asymmetric polyelectrolytes. *J. Chem. Phys.* 158:10.1063/1065.0147323.
27. SF Edwards & P Singh (1979) Size of a polymer molecule in solution. Part 1.—Excluded volume problem. *J. Chem. Soc., Faraday Trans. 2* 75:1001-1019.
28. M Muthukumar (1987) Adsorption of a polyelectrolyte chain to a charged surface. *J. Chem. Phys.* 86:7230-7235.
29. M Muthukumar (2004) Theory of counter-ion condensation on flexible polyelectrolytes: adsorption mechanism. *J. Chem. Phys.* 120:9343-9350.
30. M Muthukumar (2023) *Physics of Charged Macromolecules: Synthetic and Biological Systems* (Cambridge University Press, Cambridge).
31. A Kundagrami & M Muthukumar (2010) Effective Charge and Coil−Globule Transition of a Polyelectrolyte Chain. *Macromolecules* 43:2574-2581.
32. R Kjellander (2020) A multiple decay-length extension of the Debye–Hückel theory: to achieve high accuracy also for concentrated solutions and explain under-screening in dilute symmetric electrolytes. *Phys. Chem. Chem. Phys.* 22:23952-23985.
33. PJ Flory & WR Krigbaum (2004) Statistical Mechanics of Dilute Polymer Solutions. II. *J. Chem. Phys.* 18:1086-1094.
34. DA McQuarrie (1975) *Statistical Mechanics* (Harper & Row).
35. H Hofmann, A Soranno, A Borgia, K Gast, D Nettels, & B Schuler (2012) Polymer scaling laws of unfolded and intrinsically disordered proteins quantified with single-molecule spectroscopy. *Proc. Natl. Acad. Sci. USA* 109:16155-16160.
36. M Doi (1996) *Introduction to polymer physics* (Oxford university press).
37. K Tamiola, RM Scheek, P van der Meulen, & FAA Mulder (2018) pepKalc: scalable and comprehensive calculation of electrostatic interactions in random coil polypeptides. *Bioinformatics* 34:2053-2060.
38. MAS Hass & FAA Mulder (2015) Contemporary NMR Studies of Protein Electrostatics. *Annu. Rev. Biophys.* 44:53-75.
39. BJ Payliss, J Vogel, & AK Mittermaier (2019) Side chain electrostatic interactions and pH-dependent expansion of the intrinsically disordered, highly acidic carboxyl-terminus of γ-tubulin. *Protein Sci.* 28:1095-1105.
40. H Feng, BR Zhou, & Y Bai (2018) Binding Affinity and Function of the Extremely Disordered Protein Complex Containing Human Linker Histone H1.0 and Its Chaperone ProTalpha. *Biochemistry* 57:6645-6648.